Structural Monitoring and Maintenance, *Vol. 9, No. 3 (2022) 259-270*
https://doi.org/10.12989/smm.2022.9.3.259

Noncontact strain sensing in cement-based material using laser-induced fluorescence from nanotube-based skin

Wei Meng [1], Sergei M. Bachilo [3], Jafarali Parol [2],
R. Bruce Weisman [3,4] and Satish Nagarajaiah[*1,4,5]

[1] *Department of Civil and Environmental Engineering, Rice University, Houston, Texas, USA*
[2] *Energy and Building Research Center, Kuwait Institute for Scientific Research, Shuwaikh, Kuwait*
[3] *Department of Chemistry, Rice University, Houston, Texas, USA*
[4] *Department of Materials Science and NanoEngineering, Rice University, Houston, Texas, USA*
[5] *Department of Mechanical Engineering, Rice University, Houston, Texas, USA*

(*Received June 5, 2022, Revised August 8, 2022, Accepted September 17, 2022*)

Abstract. This study explores the use of the recently developed "strain-sensing smart skin" (S^4) method for noncontact strain measurements on cement-based samples. S^4 sensors are single-wall carbon nanotubes dilutely embedded in thin polymer films. Strains transmitted to the nanotubes cause systematic shifts in their near-infrared fluorescence spectra, which are analyzed to deduce local strain values. It is found that with cement-based materials, this method is hampered by spectral interference from structured near-infrared cement luminescence. However, application of an opaque blocking layer between the specimen surface and the nanotube sensing film enables interference-free strain measurements. Tests were performed on cement, mortar, and concrete specimens with such modified S^4 coatings. When specimens were subjected to uniaxial compressive stress, the spectral peak separations varied linearly and predictably with induced strain. These results demonstrate that S^4 is a promising emerging technology for measuring strains down to ca. 30 $\mu\varepsilon$ in concrete structures.

Keywords: concrete; near-infrared fluorescence; non-contact strain sensing; single-walled carbon nanotubes; structural health monitoring

1. Introduction

As a local damage detection and evaluation method, strain measurement is important for concrete structures to validate computational models, determine maintenance period and extend service life (Li *et al*. 2014, Colombo *et al*. 2016). Strain sensors provide direct and first-hand information on structural damage for structural health monitoring (SHM). Traditional strain sensors, such as resistance strain gauges, require physical connections to readout devices. They are stable and long-lasting but measure only at discrete locations and in individual directions, with gauge lengths of several millimeters (Obitayo and Liu 2012). New generation contact-based strain sensors, such as double-ended tuning fork gauges (Myers 2010), single- and multi-layer nanofilms fabricated using carbon nanotubes, polyelectrolyte composites (Dharap *et al*. 2004, Li *et al*. 2004,

*Corresponding author, Professor, E-mail: satish.nagarajaiah@rice.edu

http://www.techno-press.org/?journal=smm&subpage=7 ISSN: 2288-6605 (Print), 2288-6613 (Online)

Loh *et al*. 2007), and photoactive thin films (Ryu and Loh 2014), achieve high spatial resolution or strain sensitivity but still require electrical connections to the sensors for data acquisition. A noncontact carbon nanotube film strain sensor that measured strain by means of Raman spectra was first reported by Li *et al*. (2004). However, due to the low intensity of scattering signals and long measurement times, the Raman methods are not suitable for field application on large scale structures.

As an alternative to contact-based sensors, embedded sensors are also popularly used for strain and temperature monitoring in concrete structural SHM (Hill and Meltz 1997, Benedetti *et al*. 2011). Optical fiber sensors (Rodriguez *et al*. 2015) can often be embedded into structural materials. They have the advantages of providing multi-point structural strain monitoring and being immune to electromagnetic interference, but their high cost and the difficulty of deployment limit many field applications (Davis *et al*. 1997). Another novel type of embedded strain-sensing uses cement-based piezoresistive composites, in which electrical resistivity depends on strain (Chung 2000, Mirzamohammadi and Mazloom 2021). Fu and Chung (1996) found that a conductive network can be formed in concrete containing a suitable concentration of carbon fibers. Under cyclic load, damage accumulated in the concrete can be deduced from the increased resistance of the conductive network. Studies showed that this carbon filled cement-based composite sensor has an acceptable measurement precision for uniaxial compressive and tensile strain, but that it is nearly insensitive to shear strain (Xiao *et al*. 2011). Moreover, the resistance is found to also depend on humidity and temperature (Li *et al*. 2006, 2008), which significantly complicates data interpretation.

To overcome the limitations of contact-based and embedded strain sensors, a noncontact "strain-sensing smart skin" (S^4) technique using laser-induced fluorescence emission from carbon nanotubes has recently been proposed and demonstrated (Withey *et al*. 2012). Single-wall carbon nanotubes (SWCNTs) are a family of high aspect ratio tubular structures containing carbon atoms covalently bonded into specific ordered forms (Reich *et al*. 2004). SWCNT structures with different tube diameters and roll-up angles are uniquely labeled by a pair of integers, (*n*, *m*). Most of these SWCNT structural species are semiconducting. When excited with visible light, they emit fluorescence at distinct (*n*, *m*)-specific near-infrared wavelengths linked to their band gaps (O'Connell *et al*. 2002, Bachilo *et al*. 2002, Weisman and Bachilo 2003). It has been shown from theory and experiment that axial strains in SWCNTs cause systematic, predictable changes in the semiconducting band gaps and corresponding shifts in those fluorescence peak wavelengths (Yang and Han 2000, Leeuw *et al*. 2008). Thus, when SWCNTs are embedded in a film that adheres to a surface of interest, they can report local strain in the surface through spectral shifts in their emission peaks. By using polarized excitation light to measure SWCNTs emission spectra from the film at many points, one can construct a map showing strain magnitudes and directions as a function of position to detect strain concentrations and track fracture development (Sun *et al*. 2019a, b, Meng *et al*. 2022). Since there is no physical contact between the specimen and the measurement device, the instrument can be mounted on robots or drones for field application (Gucunski *et al*. 2015). Spatial resolution is approximately 0.1 mm. The current implementation of this S^4 method deduces strain based on the spectral separation between (7,5) and (7,6) SWCNT emission peaks, as shown in Fig. 1. The strain coefficient for this (7,5) − (7,6) separation is approximately 1.4 nm/mε (Sun *et al*. 2015). In this paper, we report the first efforts to extend the application of the S^4 method to measure strain in cement-based specimens.

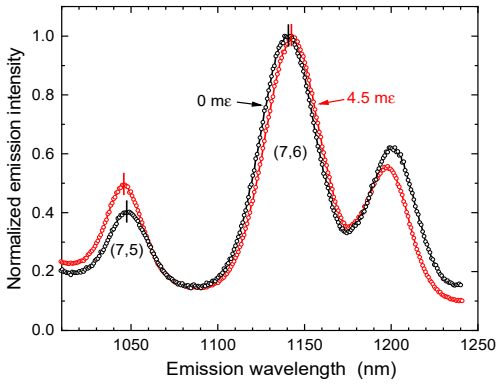

Fig. 1 Emission spectra from an S4 film on polycarbonate specimen with substrate strains of 0 (black points) and 4.5 millistrain (red points) [adapted from Sun *et al*. 2015]

2. Intrinsic emission of cement

We have found that cement, unlike metallic or polymeric specimens, emits its own intrinsic near-infrared luminescence when excited with visible light. The left panel of Fig. 2 shows the cement emission (in black) and the S^4 film emission (in red), with both excited at 660 nm. Intrinsic cement emission is an intriguing new phenomenon whose detailed characteristics is presented in a separate report (Meng *et al*. 2022). But its effect on the current project is to interfere with normal S^4 data analysis because it overlaps strongly with the SWCNT (7,6) peak and is too intense to allow accurate recovery of that (7,6) peak wavelength. However, we have been able to efficiently suppress the interfering cement emission by introducing a blocking layer between the specimen and the S^4 sensing film.

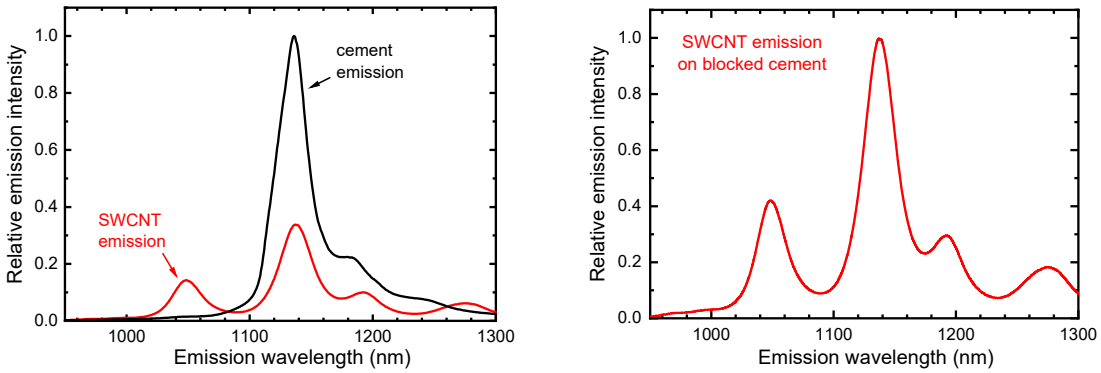

Fig. 2 Near-infrared emission spectra excited at 660 nm. Left frame: SWCNT fluorescence from S^4 film (red curve) compared to intrinsic luminescence from the cement specimen alone (black curve). Right frame: Emission measured from SWCNT strain-sensing film applied to cement specimen over blocking layer. Emission is entirely from SWCNTs, with no apparent contribution from intrinsic cement luminescence

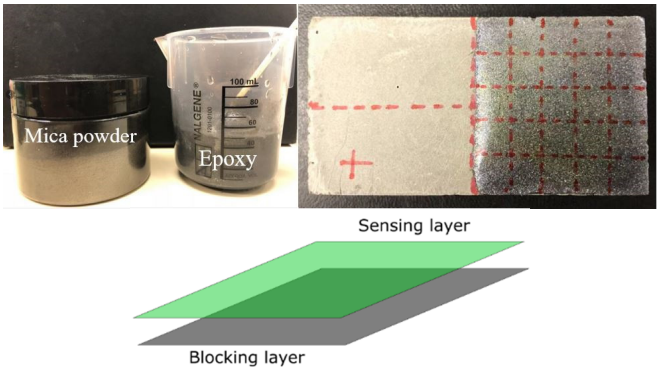

Fig. 3 Left: mica powder and epoxy used to formulate the blocking layer; Right: cement specimen with blocking layer applied to its right half. (Red dashed lines on the specimen are grids drawn used to guide scanning during tests.)

3. First generation sandwich-structured S^4 coating

3.1 Blocking layer

We tested several methods for blocking the intrinsic cement emission. A thin layer of metallic paint formed an effective optical barrier, but it was damaged during application of the toluene-based S^4 sensing layer. Another option that was explored was epoxy designed for use on cement. A product of this type made by Loctite showed good potential for blocking the interfering emission, but its coating thickness and surface roughness were difficult to control.

Another solution we found was a mixture of transparent epoxy with mica powder, as shown in Fig. 3. A 5 g portion of mica powder was mixed with 20 mL of epoxy resin and 10 mL of curing agent. The mixture was then applied by brush to form a thin coat on the cement specimen surface and cured for 48 hours. This coating was found to efficiently block the intrinsic cement emission, as can be seen in the right panel of Fig. 2. In this spectrum of an S^4 film applied over the blocking layer on cement, the intrinsic spectral component appears to be fully suppressed. Moreover, the surface of the mica/epoxy layer is smooth and reflective, which tends to enhance the S^4 optical signal.

3.2 Sensing layer

The sensing layer used in this study was based on our dual-layer S^4 film (Sun *et al*. 2019a, b). The sensing component was a submicron-thick layer of SWCNTs wrapped by the organic polymer PFO (Nish *et al*. 2007). To prepare it, solid PFO was first added to toluene at a concentration of 1 mg/mL and then dissolved by agitation with 60 min of tip ultrasonication at a power of 1 W/mL and a duty cycle of 20 s on, 20 s off. Raw SWCNTs were then added to the PFO/toluene solution at a concentration of 0.1 mg/mL and dispersed through 30 min of tip ultrasonication at the same power level and duty cycle used to prepare the PFO solution. To remove bundled nanotubes and impurities, the dispersion was centrifuged at moderate speeds for 20 min and the supernatant was collected for use as the S^4 coating material. This was applied by air-brushing onto the blocking layer of the specimen and curing to form the strain-sensing thin film.

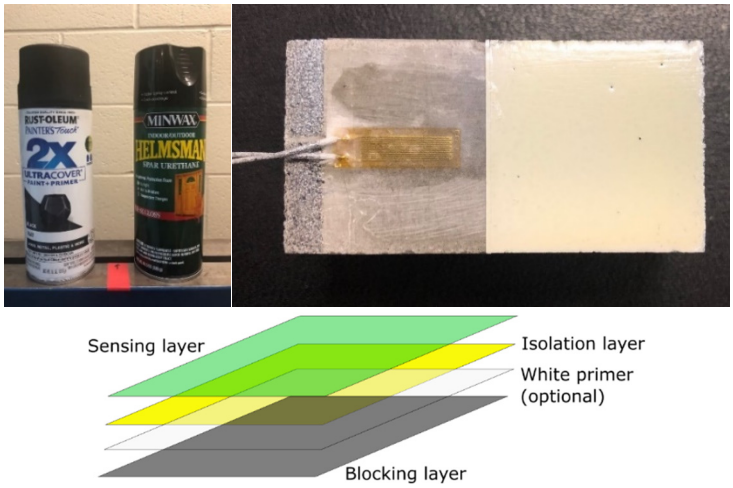

Fig. 4 Left: black paint and polyurethane sprays used to prepare the blocking and isolation layers; Right: cement specimen with the second generation S4 coating (blocking, isolation, primer, sensing, and protective overcoat) applied to its right half

4. Second generation sandwich-structured S^4 coating

During the scanning process, it was found that the surface of epoxy coating was damaged due to unintended laser-induced heating. The uneven surface caused by the laser might induce bias in the measurement result. To overcome this disadvantage, we devised another coating method to block the cement intrinsic emission.

The new coating consists of a black painted layer under a polyurethane layer. The optical barrier formed by the black paint can be damaged when the toluene-based S^4 sensing layer is applied. Therefore, an isolation layer of polyurethane was added between the blocking and sensing layer. In this way, the blocking layer is protected from solvent damage and the intrinsic cement emission remains effectively blocked. Since the blocking and isolation layers are much thinner than the epoxy layer, laser-induced heat can be quickly dissipated and the coating is not damaged during scanning. An optional white primer layer can be inserted between the blocking and isolation layers. It enhances the S^4 optical signal and reduces spatial variations in the spectral peak positions. The sensing layer is the same as described above.

Before applying the second generation S^4 coating, the surface of the cement sample needs to be cleaned by fine sandpaper and alcohol to remove dust and increase adhesion. Each layer is applied by spray and cured under ambient conditions for at least 24 hours before coating the next. The isolation layer thickness should be near 2 μm to help heat dissipation and avoid quenching effects. The final coating design is shown in Fig. 4.

5. Optical strain measurement scheme

As shown in Fig. 5, nanotubes in the S^4 film are excited with linearly polarized laser light at 660 nm, which provides near-resonant excitation for (7,5) and (7,6) SWCNT structures extracted by the organic polymer PFO. To remove weak short-wave infrared (SWIR) components, the laser

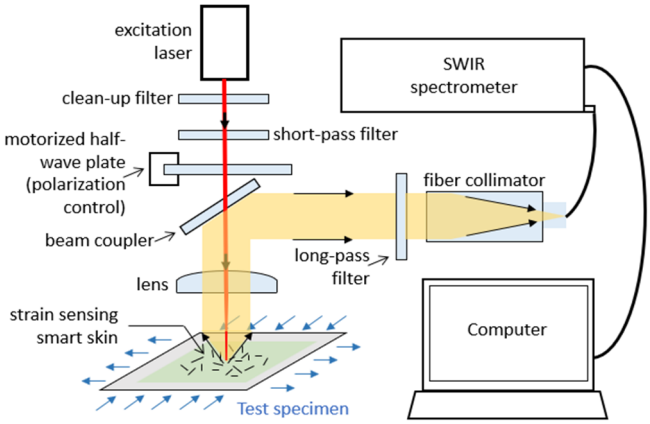

Fig. 5 Schematic diagram of S^4 strain measurement

beam first passes through a short-pass filter, then through a computer-controlled half-wave retardation plate to select a specific measurement direction by adjusting the polarization plane. After passing through a 2 mm hole in a coupling mirror, the excitation beam is focused onto the test specimen by an aspheric lens with a focal length of 11 mm. Short-wave infrared fluorescence emission from the S^4 film is captured and collimated by the same lens and then reflected by the coupling mirror to a fiber collimator connected to a SWIR spectrometer (B&W Tek Sol 1.7), which contains a thermoelectrically cooled 512 channel InGaAs detector array. The strain is deduced in real-time by a custom computer program that computes peak separations in the emission spectra and converts them to absolute strain values.

6. Experiments

The specimens used for compression tests had the dimensions 25.4 × 25.4 × 50.8 mm. They were cast from Portland Cement Type I/II with a water/cement ratio of 0.4, cement/sand ratio of 0.5 for mortar, and cement/coarse aggregate ratio of 0.3 for concrete. The sand and coarse aggregates used for specimen casting are shown in Fig. 6. The specimens were removed from the mold after 24 h, then moist-cured in water at room temperature for 7 days. Each layer described

Fig. 6 Materials for experiment concrete casting
(left: cement, middle: sand, right: sand and coarse aggregate)

above was applied to half of the specimen with an interval of 24 hours. To provide reference measurements, a conventional foil strain gauge was attached to the bare cement surface close to the S^4 coating, as shown in Fig. 4.

To acquire strain data, an S^4 reader head was substituted for the print head on a three-dimensional (3D) printer, as shown in Fig. 7. The tracking and control system enabled accurate positioning and measurement, with a computer program directing the read head to move to desired x, y and z coordinates (keeping a proper optical distance from the specimen surface) with a precision of less than 0.1 mm. This automated S^4 system raster-scanned the optical read head to a series of positions over the test specimen. The read head contained a compact 660 nm excitation laser whose polarization axis was adjusted using a computer-controlled half-wave retardation plate. The laser beam passed through optical filters, the half-wave plate, and a lens before illuminating a small region of the sample surface. The resulting SWCNT fluorescence from the S^4 film was collected, filtered, and transmitted through an optical fiber to a near-infrared spectrometer with a multichannel InGaAs detector array for capturing emission spectra. A photograph of the experimental setup is shown in Fig. 8.

The scanned region of interest (ROI) on the specimen was a 15 × 15 mm square area illustrated in Fig. 7. The read head position was scanned in steps of 0.75 mm, giving 21 data points collected along each direction, and 441 points in the whole ROI. Initially, the cement specimen was fixed in the hydraulic clamp without any applied load. The vertical read head position was adjusted for best focus on the surface, and then it was raster scanned over the ROI, acquiring the spectrum from each point in 2 seconds. For each measured spectrum, a custom data analysis program fit the peaks from (7,5) and (7,6) SWCNTs to Gaussian functions and precisely determined the spectral spacing between the two peak centers. That set of values formed the reference scan. Next, a uniaxial compressive load sufficient to give approximately 100 $\mu\varepsilon$ of strain was applied to the specimen. The test specimen was fixed on the top. The load was uniformly applied at the bottom in a quasi-static loading rate driven by a hydraulic pump. Another raster scan over the ROI was performed to obtain a new set of spectral separations between the (7,5) and (7,6) peak centers. Then the reference scan values were subtracted point-by-point from the scan values measured on the strained specimen to obtain the set of net spectral shifts. We averaged these over all 441 points to find the averaged peak shift within the ROI under load. Finally, the same procedure was repeated for different compressive loads.

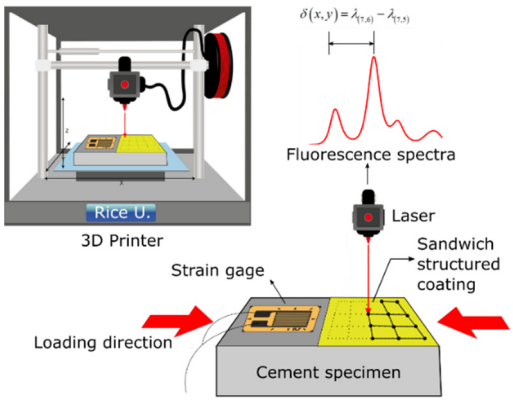

Fig. 7 Method for strain measurement testing using S^4 film sensor

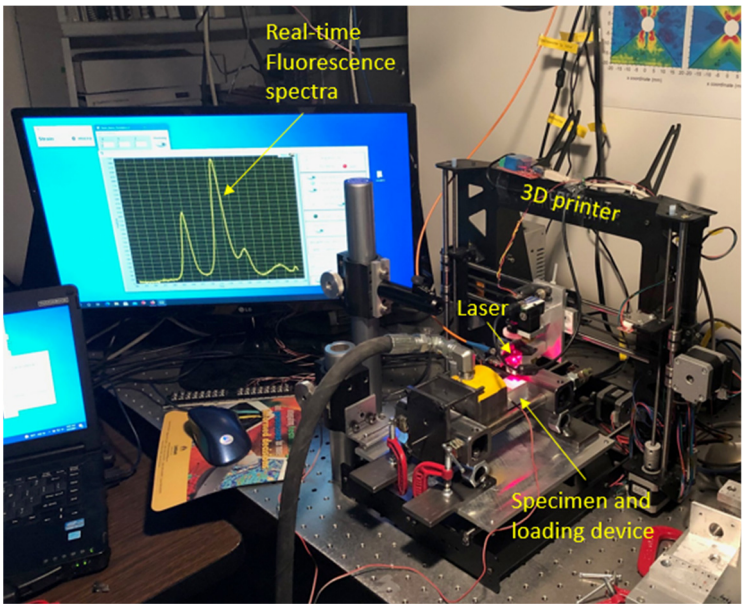

Fig. 8 Experimental apparatus for cement strain measurement using the S^4 method

7. Results

We tested three cement specimens with first-generation sandwich structured S^4 coatings subjected to different compressive loads. In addition, second-generation sandwich structured S^4 coatings were applied to cement, mortar, and concrete specimens that were compressed to the same strain level. Spectral data from the S^4 film and readings from the foil resistive strain gauge were recorded simultaneously for all runs. Figs. 9 and 10 show the averaged shifts in spectral peak separations as a function of specimen strain. The first cement specimen was strained to a maximum of ~200 $\mu\varepsilon$. The averaged spectral peak separation within the ROI increased monotonically over this range with a slope of approximately 1.6 nm/mε, indicating effective load transfer from the surface of the strained specimen to SWCNTs in the S^4 sensing layer (Sun *et al*. 2015). The second and third cement specimens were subjected to higher compressive loads. Both showed positive correlations of spectral peak separation with specimen strain, and average slopes similar to that for the first specimen. However, a significant oscillatory component appears superimposed on the linear response in these cases. We speculate that the nonlinear component may have resulted from unintended laser-induced heating of the sensing layer during scanning. Results from the other three specimens, which had second-generation sandwich structured S^4 coatings, are plotted in Fig. 10. They show much better linearity and smaller standard errors. The slope relating peak separation and applied strain was about 1.5 nm/mε, which is close to the result we obtained previously on metal specimens (Sun *et al*. 2019a, b). This consistency in slopes indicates efficient strain transmission from the cement-based substrates to the SWCNTs. The S^4 method therefore seems to be an effective new tool for measuring strains in concrete structures.

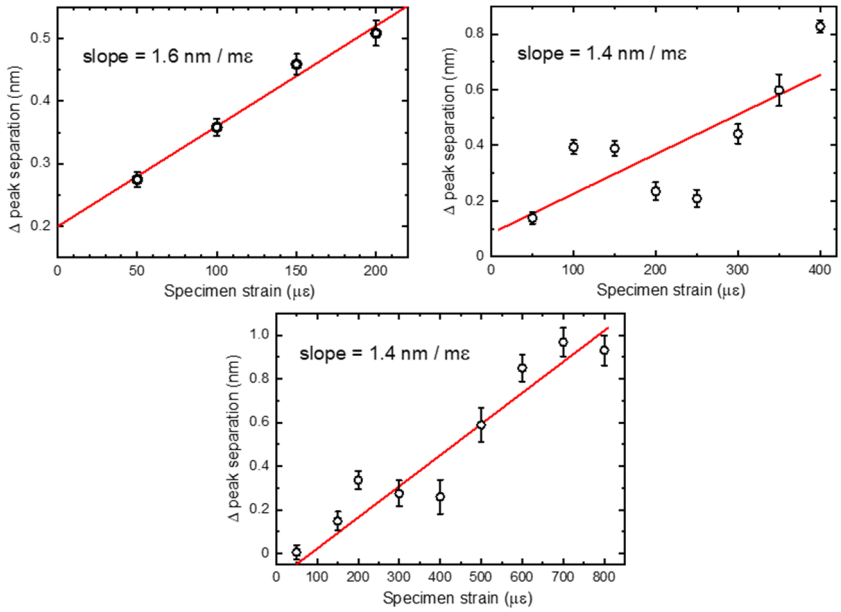

Fig. 9 First-generation coating (epoxy with mica powder as blocking layer) response of SWCNT spectral peak positions to strain in three cement specimens subjected to different peak compressive loads. Strain values were measured with foil resistance gauges. Symbols show measured values; error bars show standard errors of the means; and red lines show linear least squares fits

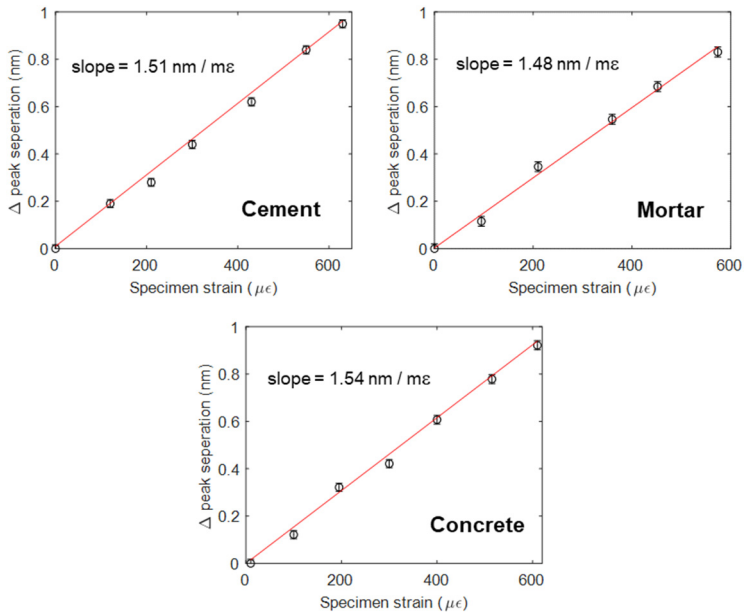

Fig. 10 Second-generation coating (primer and polyurethane coating as blocking layer) response of SWCNT spectral peak positions to compressive strain in specimens composed of cement, mortar, and concrete (as labeled). Strain values were measured with foil resistance gauges. Symbol show measured values; error bars show standard errors of the mean; and red lines show linear least squares fits

8. Conclusions

We have demonstrated the first successful use of S^4 technology for measuring strains in cement-based materials. This technology is based on the spectral response of carbon nanotube sensors and allows non-contact strain measurements over the entire specimen surface. Its use with cement-based materials is more challenging than with metals or polymers because of optical interference from previously unreported intrinsic near-infrared cement luminescence. However, we find that this interference can be efficiently blocked by a suitably formulated opaque base coating containing black paint and polyurethane. Using such modified S^4 films, we observe spectral peak shifts that correlate linearly and predictably with specimen strain. Extensions of this research will aim at using the S^4 method to measure full-field strain maps of standard concrete specimens. We expect that this noncontact optical strain measurement technology will offer a practical and valuable tool for maintaining the safety of critical concrete structures.

Acknowledgments

The authors are grateful to the Kuwait Institute of Scientific Research for research support.

References

Bachilo, S.M., Strano, M.S., Kittrell, C., Hauge, R.H., Smalley, R.E. and Weisman, R.B. (2002), "Structure-assigned optical spectra of single-walled carbon nanotubes", *Sci*., **298**(5602), 2361-2366. https://doi.org/10.1126/science.1078727

Benedetti, M., Fontanari, V. and Zonta, D. (2011), "Structural health monitoring of wind towers: remote damage detection using strain sensors", *Smart Mater. Struct*., **20**(5), 1-13. https://doi.org/10.1088/0964-1726/20/5/055009

Chung, D.D.L. (2000), "Cement reinforced with short carbon fibers: a multifunctional material", *Compos. Part B*: *Eng*., **31**(6-7), 511-526. https://doi.org/10.1016/S1359-8368(99)00071-2

Colombo, M., Domaneschi, M. and Ghisi, A. (2016), "Existing concrete dams: loads definition and finite element models validation", *Struct. Monitor. Maint., Int. J*., **3**(2), 129-144. https://doi.org/10.12989/smm.2016.3.2.129

Davis, M.A., Bellemore, D.G. and Kersey, A.D. (1997), "Distributed fiber Bragg grating strain sensing in reinforced concrete structural components", *Cement Concrete Compos*., **19**(1), 45-57. https://doi.org/10.1016/s0958-9465(96)00042-x

Dharap, P., Li, Z., Nagarajaiah, S. and Barrera, E.V. (2004), "Nanotube film based on single-wall carbon nanotubes for strain sensing", *Nanotechnology*, **15**(3), 379-382. https://doi.org/10.1088/0957-4484/15/3/026

Fu, X. and Chung, D.D.L. (1996), "Self-monitoring of fatigue damage in carbon fiber reinforced cement", *Cement Concrete Res*., **26**(1), 15-20. https://doi.org/10.1016/0008-8846(95)00184-0

Gucunski, N., Kee, S., La, H., Basily, B. and Maher, A. (2015), "Delamination and concrete quality assessment of concrete bridge decks using a fully autonomous RABIT platform", *Struct. Monitor. Maint*., *Int. J*., 2(1), 19-34. http://doi.org/10.12989/smm.2015.2.1.019

Hill, K.O. and Meltz, G. (1997), "Fiber Bragg grating technology fundamentals and overview", *J. Lightwave Technol*., **15**(8), 1263-1276.https://doi.org/10.1109/50.618320

Leeuw, T.K., Tsyboulski, D.A., Nikolaev, P.N., Bachilo, S.M., Arepalli, S. and Weisman, R.B. (2008), "Strain measurements on individual single-walled carbon nanotubes in a polymer host: structure-dependent spectral shifts and load transfer", *Nano Letters*, **8**(3), 826-831.

https://doi.org/10.1021/nl072861c
Li, Z., Dharap, P., Nagarajaiah, S., Barrera, E.V. and Kim, J.D. (2004), "Carbon nanotube film sensors", *Adv. Mater.*, **16**(7), 640-643. https://doi.org/10.1002/adma.200306310
Li, H., Xiao, H.G. and Ou, J.P. (2006), "Effect of compressive strain on electrical resistivity of carbon black-filled cement-based composites", *Cement Concrete Compos.*, **28**(9), 824-828. https://doi.org/10.1016/j.cemconcomp.2006.05.004
Li, H., Xiao, H. and Ou, J. (2008), "Electrical property of cement-based composites filled with carbon black under long-term wet and loading condition", *Compos. Sci. Technol.*, **68**(9), 2114-2119. https://doi.org/10.1016/j.compscitech.2008.03.007
Li, H.N., Yi, T.H., Ren, L., Li, D.S. and Huo, L.S. (2014), "Reviews on innovations and applications in structural health monitoring for infrastructures", *Struct. Monitor. Maint., Int. J.*, **1**(1), 1-45. https://doi.org/10.12989/smm.2014.1.1.001
Loh, K.J., Kim, J., Lynch, J.P., Kam, N.W.S. and Kotov, N.A. (2007), "Multifunctional layer-by-layer carbon nanotube–polyelectrolyte thin films for strain and corrosion sensing", *Smart Mater. Struct.*, **16**(2), 429-438. https://doi.org/10.1088/0964-1726/16/2/022
Meng, W., Pal, A., Bachilo, S.M., Weisman, R.B. and Nagarajaiah, S. (2022), "Next-generation 2D optical strain mapping with strain-sensing smart skin compared to digital image correlation", *Scientific Reports*, **12**(1), 1-12. https://doi.org/10.1038/s41598-022-15332-1
Meng, W., Bachilo, S.M., Parol, J., Nagarajaiah, S. and Weisman, R.B. (2022), "Near-infrared photoluminescence of Portland cement", *Scientific Reports*, **12**(1), 1-6. https://doi.org/10.1038/s41598-022-05113-1
Mirzamohammadi, S. and Mazloom, M. (2021), "Monitoring the required energy for the crack propagation of fiber-reinforced cementitious composite", *Struct. Monitor. Maint., Int. J.*, **8**(3), 279-294. https://doi.org/10.12989/smm.2021.8.3.279
Myers, D.R. (2010), "MEMS Resonant Strain Sensor Integration", Ph.D. Dissertation, University of California, Berkeley, CA, USA.
Nish, A., Hwang, J.Y., Doig, J. and Nicholas, R.J. (2007), "Highly selective dispersion of single-walled carbon nanotubes using aromatic polymers", *Nature Nanotechnol.*, **2**(10), 640-646. https://doi.org/10.1038/nnano.2007.290
Obitayo, W. and Liu, T. (2012), "A review: carbon nanotube-based piezoresistive strain sensors", *J. Sensors*, 2012. https://doi.org/10.1155/2012/652438
O'connell, M.J., Bachilo, S.M., Huffman, C.B., Moore, V.C., Strano, M.S., Haroz, E.H., Rialon, K.L., Boul, P.J., Noon, W.H., Kittrell, C. and Ma, J. (2002), "Band gap fluorescence from individual single-walled carbon nanotubes", *Science*, **297**(5581), 593-596. https://doi.org/10.1126/science.1072631
Reich, S., Thomsen, C. and Maultzsch, J. (2004), *Carbon Nanotubes*: *Basic Concepts and Physical Properties*, John Wiley & Sons.
Rodriguez, G., Casas, J.R. and Villalba, S. (2015), "SHM by DOFS in civil engineering: A review", *Struct. Monitor. Maint., Int. J.*, **2**(4), 357-382. https://doi.org/10.12989/smm.2015.2.4.357
Ryu, D. and Loh, K.J. (2014), "Multi-modal sensing using photoactive thin films", *Smart Mater. Struct.*, **23**(8), 085011. https://doi.org/10.1088/0964-1726/23/8/085011
Sun, P., Bachilo, S.M., Weisman, R.B. and Nagarajaiah, S. (2015), "Carbon nanotubes as non-contact optical strain sensors in smart skins", *J. Strain Anal. Eng. Des.*, **50**(7), 505-512. https://doi.org/10.1177/0309324715597414
Sun, P., Bachilo, S.M., Lin, C.W., Weisman, R.B. and Nagarajaiah, S. (2019a), "Noncontact strain mapping using laser-induced fluorescence from nanotube-based smart skin", *J. Struct. Eng.*, (1), 04018238, 1-20. https://doi.org/10.1061/(ASCE)ST.1943-541X.0002227
Sun, P., Bachilo, S.M., Lin, C.W., Nagarajaiah, S. and Weisman, R.B. (2019b), "Dual-layer nanotube-based smart skin for enhanced noncontact strain sensing", *Struct. Control Health Monitor.*, **26**(1), e2279, 1-11. https://doi.org/10.1002/stc.2279
Weisman, R.B. and Bachilo, S.M. (2003), "Dependence of optical transition energies on structure for single-walled carbon nanotubes in aqueous suspension: an empirical Kataura plot", *Nano Letters*, **3**(9), 1235-

1238. https://doi.org/10.1021/nl034428i

Withey, P.A., Vemuru, V.S.M., Bachilo, S.M., Nagarajaiah, S. and Weisman, R.B. (2012), "Strain paint: Noncontact strain measurement using single-walled carbon nanotube composite coatings", *Nano Letters*, **12**(7), 3497-3500. https://doi.org/10.1021/nl301008m

Xiao, H., Li, H. and Ou, J. (2011), "Strain sensing properties of cement-based sensors embedded at various stress zones in a bending concrete beam", *Sensors Actuators A*: *Phys*., **167**(2), 581-587. https://doi.org/10.1016/j.sna.2011.03.012

Yang, L. and Han, J. (2000), "Electronic structure of deformed carbon nanotubes", *Phys*. *Rev*. *Lett*., **85**(1), 154-157. https://doi.org/10.1103/PhysRevLett.85.154

JK